Chemical Science

ROYAL SOCIETY OF CHEMISTRY

EDGE ARTICLE

View Article Online
View Journal | View Issue

Cite this: *Chem. Sci.*, 2023, **14**, 1132

All publication charges for this article have been paid for by the Royal Society of Chemistry

Received 7th November 2022
Accepted 27th December 2022

DOI: 10.1039/d2sc06151a

rsc.li/chemical-science

A decacationic ferrocene-based metallostar†

Susanne Margot Rupf, Amina Leoni Moshtaha and Moritz Malischewski *

Decacationic metallostars have been prepared by the reaction of permercurated ferrocene $FeC_{10}(HgO_2CCF_3)_{10}$ with superacidic $(C_5F_5NH)(SbF_6)$ ($pK_a = -11$ estimated in H_2O) in multigram scale. In the resulting compound, $[FeC_{10}Hg_{10}(NC_5F_5)_n][SbF_6]_{10}$, the labile pentafluoropyridine ligands are readily displaced by acetonitrile (MeCN) or tetrahydrothiophene (THT). In the X-ray structure of $[FeC_{10}Hg_{10}(THT)_{10}][SbF_6]_{10}\cdot 24$ MeCN no cation–anion contacts between mercury and fluorine were observed. Moreover, cyclic voltammetry measurements of $[FeC_{10}(Hg(MeCN))_{10}]^{10+}$ and $[FeC_{10}(Hg(THT))_{10}]^{10+}$ revealed a (quasi)reversible one-electron oxidation of Fe(II) to Fe(III). From the reaction of $[FeC_{10}(Hg(MeCN))_{10}]^{10+}$ with MoF_6 as oxidant the ferrocenium cation $[FeC_{10}(Hg(MeCN))_{10}]^{11+}$ was obtained and characterized *via* single crystal XRD. These electrophilic metallostars are promising potential building blocks for the synthesis of dendritic architectures containing a robust, tenfold functionalized ferrocene core.

Introduction

The relevance of biological redox processes of metalloproteins for living organisms inspired chemists to design redox active macromolecular compounds.[1] In this context the functionalization of dendrimers with redox active building blocks has received considerable attention as they are well defined macromolecules in terms of size and peripheral chemical functionality.[2] In the last decades these dendrimers have found applications as multielectron redox catalysts as well as reservoirs, in the surface modification of electrodes or in electrochemical sensors.[3,4] Their molecular architecture often resembles star-shaped structures with a core and different ligand building blocks which are not limited to organic moieties but also include examples of p-block and metal(organic) fragments.[5] A widely used redox active building block is the ferrocenyl group due to the reversibility of the $Fe^{+II/+III}$ redox couple and the high thermal stability of the oxidized and the native form in particular.[6] In many molecular stars the metallocene unit is located in the outskirts of the molecule[7–22] despite its C_5 symmetry rendering it as an ideal core building block. Examples of ferrocene centered metallostars are rare[23,24] probably due to the synthetic difficulties associated with the poly- or perfunctionalization of ferrocene.[25]

In 2021 we reported a simple perfunctionalization approach by treatment of ferrocene with mercury(II) carboxylates to obtain $FeC_{10}(HgX)_{10}$ (X = $O_2CC_3H_7$, O_2CCF_3, O_2CCCl_3) in multigram scale.[26] Although these compounds offer relatively weak Hg–C bonds allowing transmetallation[27,28] and electrophilic substitution reactions[29,30] they are chemically inert towards air and strong Brønsted acids (*e.g.* CF_3CO_2H $pK_a = -2.7$ estimated in H_2O[31]) caused by the low polarity of the Hg–C bond as well as the low Lewis acidity of the R–Hg–X units to form adducts with increased coordination number.[32] Higher coordination numbers are usually observed in organomercury compounds with electron deficient substituents,[33–35] as shown by the Gabbaï group for [*o*-$(HgC_6F_4)_3$] which forms supramolecular architectures with aromatic hydrocarbons[36,37] or weak Lewis acid/base adducts with a variety of O, N, P and S donors.[38–40] In contrast

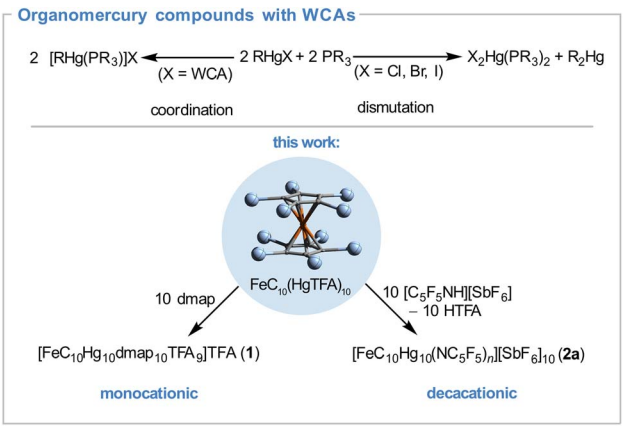

Scheme 1 Reactivity of cationic organomercury compounds towards neutral ligand like phosphine[41–44] and pyridine derivatives (this work) in presence of weakly coordinating anions (WCA). WCA = ClO_4^-, NO_3^-.[41–43]

Freie Universität Berlin, Fabeckstr. 34-36, 14195 Berlin, Germany. E-mail: moritz.malischewski@fu-berlin.de

† Electronic supplementary information (ESI) available. CCDC 2214089, 2213962 and 2213956. For ESI and crystallographic data in CIF or other electronic format see DOI: https://doi.org/10.1039/d2sc06151a

to this, in polar organomercury compounds R–Hg–X the anionic groups can be displaced by neutral ligands, *e.g.* phosphines, to give $[RHg(PR_3)]X$ (Scheme 1) maintaining the linear two-fold coordination.[41–43] The resulting cation $[RHg(PR_3)]^+$ is stable in presence of weakly coordinating anions (*e.g.* $X = ClO_4^-$) but dismutates in presence of halides ($X = Cl^- < Br^- < I^-$).[44] We envisioned that the displacement of anionic ligands in permercurated ferrocenes $FeC_{10}(HgX)_{10}$ would lead to the formation of highly charged species. Moreover, such polycations should be ideal precursors for ferrocene centered metallostars since they offer accessible coordination sites with predominantly linear coordination around the mercury atoms.

Results and discussion

$FeC_{10}(HgO_2CCF_3)_{10}$ was dissolved in tetrahydrofuran and an excess of 4-(dimethylamino)pyridine (dmap) was added (Scheme 1) yielding an orange precipitate. The solid was analysed by NMR and vibrational spectroscopy as well as elemental analysis. While the IR spectrum of the coordination compound exhibits bands which correspond only to the trifluoroacetate[45] (TFA) as well as the nitrogen based ligand,[46] the Raman spectrum features further information especially with respect to the metallocene framework. C^{Cp}–C^{Cp} deformation is found at $\tilde{\nu} = 951\ cm^{-1}$ and Hg–Cp vibrations at $\tilde{\nu} = 100\ cm^{-1}$. Moreover, the Hg–$O^{TFA}$ band ($\tilde{\nu} = 311\ cm^{-1}$ in $FeC_{10}(HgTFA)_{10}$) vanished and new bands at $\tilde{\nu} = 193–158\ cm^{-1}$ appeared, indicating the successful replacement of the carboxylic ligands by the pyridine analogues. ^1H, ^{19}F and ^{13}C NMR signals show the intact ligands and anions but as in the starting material the ^{199}Hg resonance is not visible. The coordination to the mercury atoms causes a low field shift of $\Delta\delta = 6$ ppm of the C^{Cp} signals in the ^{13}C NMR spectrum while all other signals are not significantly affected. The composition was determined by elemental analysis yielding the overall formula $FeC_{10}Hg_{10}dmap_{10}TFA_{10}$ (**1**).

Single crystals were obtained by recrystallization from tetrahydrofuran. Compound **1** crystallized in the monoclinic space group $P2_1/n$ containing one metallocene molecule in the asymmetric unit. All mercury atoms are almost linearly coordinated by one cyclopentadienyl and one dmap ligand with angles of 167.0(3)–178.6(4)° (Table 1), respectively. The distortion from linearity is caused by Hg–O^{TFA} interactions within the sum of van der Waals radii of mercury ($r_{vdW} = 1.75$ Å)[47] and oxygen ($r_{vdW} = 1.52$ Å).[48] The Hg–O distances display a broad range of 2.24(1)–3.28(4) Å and are longer than in $FeC_{10}(HgO_2CCF_3)_{10}$ (Table 1). The TFA anions serve as bridging ligands between two to three metal centers (Fig. 1A) similarly to the structure of $Hg(TFA)_2 \cdot 2$ dmap which crystallizes as a dimer bridged by two TFA anions with a distorted octahedral coordination environment around the mercury atoms.[46] This coordination motif causes an eclipsed conformation in **1a** ($Cp^{torsion} = 3.6(1)°$) in contrast to $FeC_{10}(HgO_2CCF_3)_{10}$ which exhibits a staggered conformation in solid state. As a result, one intramolecular Hg–Hg contact of 3.440(2) Å is observed. Taking all interactions into account the total coordination number of the mercury atoms is four to six. As only two non-coordinating (distorted) TFA units within the

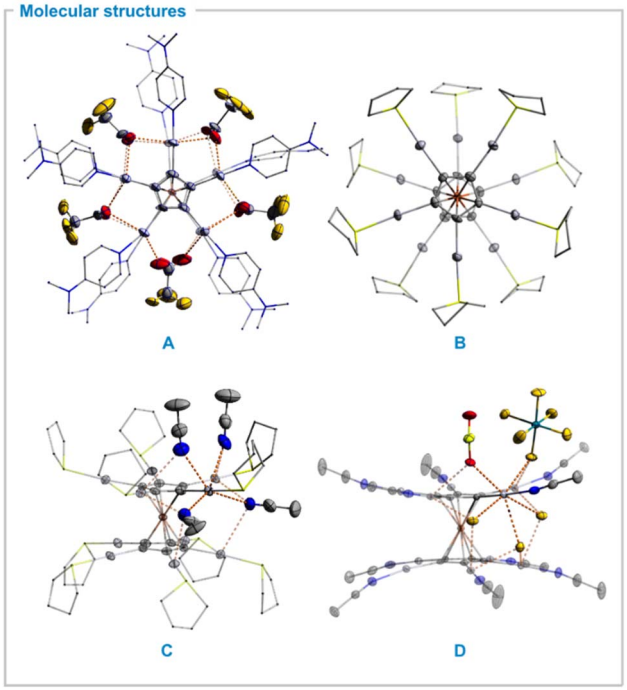

Fig. 1 Molecular structures of selected star-shaped permercurated metallocene cations in solid state. Ellipsoids with 50% probability level. Color code: mercury – light grey, antimony – turquoise, iron – orange, sulfur – neon yellow, fluorine – yellow, oxygen – red, nitrogen – blue, carbon – dark grey. Metal-anion or solvent interactions are shown as dashed orange lines. Hydrogen atoms, selected solvents and counter anions as well as disorder is omitted for clarity. (A) Inner sphere coordination of bridging TFA anions in $FeC_{10}Hg_{10}dmap_{10}(O_2CCF_3)_{10}$. (B) $[FeC_{10}(HgTHT)_{10}]^{10+}$ molecular fragment. (C) Solvent coordination motif in $[FeC_{10}(HgTHT)_{10}]^{10+}$ structure. (D) $[FeC_{10}(HgMeCN)_{10}]^{11+}$ molecular fragment as well as coordination of selected solvents and counter anion.

Table 1 Selected bond distances [Å] and angles [°] within the sum of van der Waals radii

Compound	$FeC_{10}(HgO_2CCF_3)_{10}$[26] ($X = O^{TFA}$)	**1a** ($X = O^{TFA}$)	**2b** ($X = S^{THT}$)	**2c[MoF_6]** ($X = N^{MeCN}$)
Fe–Cp^{center}	1.660(1)	1.672(2)	1.651(1), 1.658(1)	1.738(1)
Hg–C	2.034(9)–2.040(8)	2.009(10)–2.062(8)	2.022(10)–2.046(9)	2.023(6)–2.039(7)
Hg–X	2.082(7)–2.115(6)	2.241(17)–3.286(36)	2.395(2)–2.405(2)	2.050(6)–2.062(5)
$Hg–Hg^{intramol.}$	—	3.440(2)	—	—
C–Hg–X	168.8(3)–176.5(3)	167.0(3)–178.6(4)	170.8(2)–176.7(2)	171.2(3)–175.1(2)
Conformation	Staggered	Eclipsed	Staggered	Staggered

unit cell with an overall occupancy of 1.33 are observed, this metallocene is better described as a "monocation" $[FeC_{10}(HgdmapH)_{10}(TFA)_{8.66}][TFA]_{1.33}$.

In order to reduce cation anion interactions, we introduced more weakly coordinating anions by protonation of the TFA anions with protonated pentafluoropyridine $[C_5F_5NH][SbF_6]$ ($pK_a \approx -11$ estimated in H_2O[49]) in liquid SO_2 (Scheme 1) yielding $[FeC_{10}Hg_{10}(NC_5F_5)_n][SbF_6]_{10}$ (**2a**) quantitatively as an insoluble orange solid whereas trifluoroacetic acid can be removed in vacuum. The completeness of the protonation was confirmed by the absence of TFA vibrations in the corresponding IR as well as Raman spectra (Fig. S7†). Instead, additional Sb–F bands are present at $\tilde{\nu} = 660$ and 633 cm^{-1} in the infrared spectrum as well as C–C and C–F vibrations in the Raman and infrared spectrum which could be assigned to C_5F_5N[50] indicating coordination to the metal center. Protodemercuration is negligible as neither ν(Cp–H) in the 3100 cm^{-1} region nor (intense) δ(Cp–H) vibrations in the 1100 cm^{-1} region are visible in both spectra which again confirms the stability of the Cp–Hg bonds. Unfortunately, the total composition could not be determined by elemental analysis due to the sensitivity of the compound.

Substitution of the C_5F_5N ligands improves the solubility of the corresponding compounds considerably and enables the full characterization of the compounds $[FeC_{10}(Hg solv.)_{10}][SbF_6]_{10}$ (solv. = tetrahydrothiophene (THT) **2b**, MeCN **2c**). Both metallocenes show similar features in the vibrational spectra as discussed for compound **2a**. The C^{Cp} signals in the ^{13}C NMR spectra ($\delta = 111.8$ (**2b**) and 97.7 ppm (**2c**)) are again low field shifted in comparison to the signal of $FeC_{10}(HgTFA)_{10}$ as shown for compound **1**, previously.

Single crystals of the THT-complex **2b**·24 MeCN were obtained upon recrystallization from acetonitrile at −30 °C. It crystallized in the space group *C*2/*c*. The asymmetric unit contains a $\{Fe(CHgTHT)_5\}$ fragment with the iron position located at a center of inversion. The Cp ligands are aligned in a staggered conformation with torsion angles between 30.3(4) and 34.1(4)° (Fig. 1B). Again, the mercury atoms are linearly coordinated by a cyclopentadienyl and a THT ligand. In contrast to the structure of **1** no mercury anion contacts are visible (Fig. 1C). Instead, the decacationic fragment $[FeC_{10}(HgTHT)_{10}]^{10+}$ is fully solvated by 20 acetonitrile molecules. Ten of those are coordinating systematically two to three different mercury atoms from the space within both Cp rings and the other ten from the outer-sphere of the metallocene framework yielding a distorted octahedral geometry for all mercury atoms. The Hg–N distances are in range of 2.941(8)–3.289(8) Å. The interactions between cations and anions are mainly a consequence of hydrogen bonding to the solvent as well as the THT ligand. A detailed discussion of the packing motif of the decacation (**2b**) can be found in the ESI.†

Since $[FeC_{10}(HgTHT)_{10}][SbF_6]_{10}$ can be regarded as a ferrocene with ten cationic $[Hg(THT)]^+$ substituents the oxidation potentials of the metallocene are expected to be higher than in unsubstituted ferrocene as similar observations were reported for a series of acceptor substituted metallocenes.[51] Herein, Sundermeyer *et al.* observed increasing oxidation potentials of up to $\Delta E = 474$ mV per cationic group $\{SR_2\}^+$ group. The electrochemical properties of the compounds **1** and **2b,c** were determined by cyclic voltammetry. Unfortunately, the metallocene **1** decomposed upon oxidation preventing the determination of the oxidation potentials. The measurements of the soluble decacationic THT and MeCN complexes **2b** and **2c** were performed in acetonitrile and referenced against the FcH/FcH^+ redox couple (Fig. 2). Both compounds exhibit a reversible one-electron oxidation of the redox couple $Fe^{+II/+III}$ at $E_{1/2}{}^{THT} = 0.522$ V and $E_{1/2}{}^{MeCN} = 0.713$ V as well as irreversible oxidations above $E_a > 1.3$ V (Fig. S24 and S25, ESI†). The comparison of the $Fe^{+II/+III}$ potentials with the starting material $FeC_{10}(HgTFA)_{10}$ ($E_{1/2} = 0.450$ V) shows increasing oxidation potentials depending on the coordination strength of the ligand (TFA > THT > MeCN). Therefore, $[FeC_{10}Hg_{10}(NC_5F_5)_n][SbF_6]_{10}$, is expected to exhibit the highest oxidation potential in the series TFA < THT < MeCN < NC_5F_5 although its insolubility prevented its electrochemical characterization. A similar trend was already observed in Ag(I) compounds which vary enormously in oxidation potentials depending on the ligands at the metal center or simply the solvation ability of the solvents.[52] The surprisingly low potentials of the 10+/11+ redox couple are probably a consequence of the large size and effective solvation of these highly charged species as in multicationic ferrocenyl dendrimers.[53]

To realise the chemical oxidation of the permercurated ferrocene decacations we used different moderate oxidants in liquid SO_2 which allow solely oxidation to the desired ferrocenium compounds. The oxidations were tested with $Ag[SbF_6]$, $NO[BF_4]$, $NO_2[SbF_6]$ as well as MoF_6. Unfortunately, the presence of coordinating ligands seemed to reduce the reactivity of silver salts as no reaction of none of the compounds was observed with $AgSbF_6$. Moreover, $[FeC_{10}Hg_{10}(NC_5F_5)_n][SbF_6]_{10}$

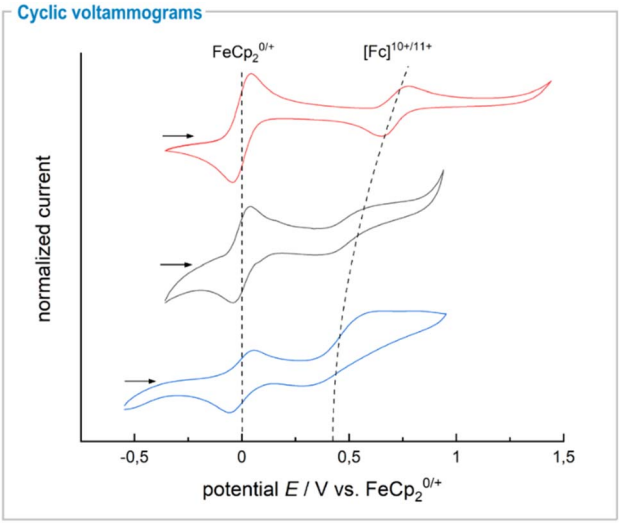

Fig. 2 Cyclic voltammograms of compounds $FeC_{10}(HgO_2CCF_3)_{10}$ in THF with 0.1 M $TBAPF_6$ as supporting electrolyte (bottom),[26] $[FeC_{10}(HgTHT)_{10}][SbF_6]_{10}$ (**2b**, middle) and $[FeC_{10}(HgMeCN)_{10}][SbF_6]_{10}$ (**2c**, top) in acetonitrile without supporting electrolyte at 100 mV s^{-1} scan rate and room temperature.

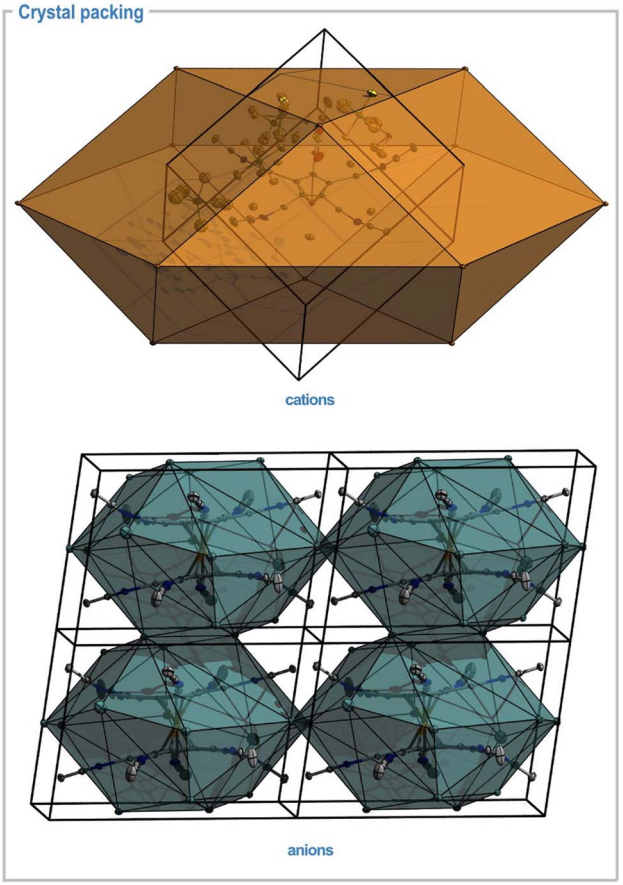

Fig. 3 Packing motifs of anions and cations in the crystal structure of $[FeC_{10}Hg(MeCN)_{10}][SbF_6]_{10}[MoF_6]$ 2 SO_2·10 HF. Top: asym. unit and closest iron positions forming a cuboctahedron. Bottom: four units cells containing heavy metal positions forming distorted square orthobicupolas around the undecacation. Ellipsoids drawn with 50% probability level. Color code: mercury – light grey, molybdenum – purple, antimony – turquoise, iron – orange, sulphur – neon yellow, fluorine – yellow, oxygen – red, carbon – dark – grey.

showed no reaction with $(NO)^+$ but with $(NO_2)^+$ indicating high oxidation potentials which perfectly fits to the correlation between ligand strength and redox potential. Reactions with $(NO_2)^+$ and MoF_6 were successful in all cases.

Single crystals of **2c[MoF$_6$]**·10 HF·2 SO_2 were obtained upon recrystallisation from HF/SO_2 at −74 °C. The compound crystallized in the space group $P\bar{1}$. The asymmetric unit consists of one $\{FeC_5(HgMeCN)_5\}$ moiety with a center of inversion located at the iron atom. The oxidation of the iron center is indicated by an elongated iron-cyclopentadienyl distance of 1.738(1) Å which is in the same order of magnitude as other substituted ferrocenium salts but significantly longer than those of non-substituted ferrocenium cations.[54] The metallocene cation is again fully solvated by 10 HF molecules with Hg–F^{HF} distances of 2.817(5)–2.956(4) Å within the inner-sphere of the metallocene framework in a similar fashion as discussed for compound **2b** triggering a staggered conformation with torsion angles in the range of 31.1(1)° to 35.9(1). However, the structure features several additional Hg–F cation–anion interactions of 2.824(5)–3.090(5) Å length yielding a coordination number of four to six for all mercury atoms (Fig. 1D). The Hg–F contacts to the $[SbF_6]^-$ counter anions are present due to the low solvation of the undecacation in HF, in contrast to the THT complex **2b** which was recrystallized from acetonitrile.

Both, the solid-state structure of $[FeC_{10}(HgTHT)_{10}]^{10+}$ and $[FeC_{10}(HgMeCN)_{10}]^{11+}$ are rare examples of isolated organometallic deca- and undecacations. Although the large variety of multicationic organic or organometallic compounds,[55–60] only a few examples for crystallographically characterized octa-,[61] nona-,[62] deca-,[63–65] dodeca[66] and even hexadecacations[67] have been reported in the past years. In such multications, the positive charges are kinetically stabilized by organic ligands *via* formation of large aggregates.[68] These so-called "lipophilically wrapped polyion aggregates" are usually not perfectly spheric causing voids within the crystal packing. Therefore, the formation of a closest packing arrangements or typical structure types as observed for (pseudo-)spherical components of low charge is prevented. In the crystal structure of $[FeC_{10}Hg(MeCN)_{10}][SbF_6]_{10}[MoF_6]\cdot 2\ SO_2\cdot 10$ HF the iron atoms produce a distorted hexagonal distorted arrangement along the [111] direction but with a ABC-stacking pattern similar to the face-centered cubic structure of copper causing a distorted cuboctahedral geometry around each iron position (Fig. 3, top). Considering only the centers of gravity for all molecular entities, no simple packing arrangement is observed for the anionic units. The undecacation is surrounded by 16 anions in a distorted square orthobicupolar geometry (Fig. 3, bottom). These polyhedra are edge-sharing with the same polyhedra of adjacent unit cells along *a* and *b* and corner-sharing along *c* resulting in a 1 : 11 composition of cations and anions. Sulphur moieties from SO_2 solvates are capping two adjacent faces on both apical sides of the bicupolas.

Conclusions

In summary, we investigated the reactivity of permercurated ferrocene derivatives towards neutral ligands in standard organic solvents as well as in superacidic medium.[69] We demonstrated that in the compound $FeC_{10}(HgTFA)_{10}$ all mercury atoms are accessible to Lewis bases. The Lewis acidity of the $\{FeC_{10}Hg_{10}\}^{10+}$ framework was tuned by variation of the counter anions. While the TFA salt only binds to strong σ-donors like dmap, the presence of weakly coordinating anions allows to isolate solvent adducts $[FeC_{10}(HgL)_{10}][SbF_6]_{10}$ (with L = C_5F_5N, MeCN, THT). Surprisingly, in those compounds the Hg–C bonds are inert to Brønsted acids, such as $[C_5F_5NH][SbF_6]$. Moreover, we report the preparation of undecacations $[FeC_{10}(HgMeCN)_{10}]^{11+}$ and $[FeC_{10}(HgTHT)_{10}]^{11+}$ as stable solids. Both, the solid-state structure of $[FeC_{10}(HgTHT)_{10}]^{10+}$ and $[FeC_{10}(HgMeCN)_{10}]^{11+}$ are rare examples of isolated organometallic deca- and undecacations.[70] The combination of the accessible coordination sites, electrochemical properties as well as their reliable multigram synthesis renders these

deca- and undecacations as promising precursors for even larger star-shaped molecular architectures (*e.g.* dendrimers).

Data availability

Besides the ESI† and the crystal structures in CCDC we have not deposited any data in other repositories.

Author contributions

The project was developed by S. M. R. and M. M. Both authors wrote the manuscript with main contributions from S. M. R. The synthetic work was carried out by S. M. R. and A. L. M, S. M. R. performed cyclic voltammetry and UV/vis experiments as well as measured and solved the SCXRD data. A. L. M. performed further NMR, IR and Raman experiments and prepared the single crystals.

Conflicts of interest

There are no conflicts to declare.

Acknowledgements

Gefördert durch Deutsche Forschungsgemeinschaft (DFG) – Projektnummer: 387284271 – SFB 1349. Funded by Deutsche Forschungsgemeinschaft (DFG) – project number: 387284271 – SFB 1349. Computing time was made available by High-Performance Computing at ZEDAT/FU Berlin. We would like to acknowledge the assistance of the Core Facility BioSupraMol supported by the DFG. The authors thank Prof. Dr Florian Kraus (Philipps-Universität Marburg) and Dr Günther Thiele (Freie Universität Berlin) for helpful discussions.

Notes and references

1 D. Astruc, *J. Leather Sci. Eng.*, 2020, **2**, 1–17.
2 C. Gorman, *Adv. Mater.*, 1998, **10**, 295–309.
3 D. Astruc, C. Ornelas and J. Ruiz, *Acc. Chem. Res.*, 2008, **41**, 841–856.
4 G. R. Newkome, E. He and C. N. Moorefield, *Chem. Rev.*, 1999, **99**, 1689–1746.
5 H. Detert, M. Lehmann and H. Meier, *Materials*, 2010, **3**, 3218–3330.
6 D. Astruc, *Eur. J. Inorg. Chem.*, 2017, 6–29.
7 B. Kayser, J. Altman, H. Nöth, J. Knizek and W. Beck, *Eur. J. Inorg. Chem.*, 1998, 1791–1798.
8 M. Iyoda, T. Kondo, T. Okabe, H. Masuyama, S. Sasaki and Y. Kuwatani, *Chem. Lett.*, 1997, **26**, 35–36.
9 R. Misra, R. Maragani, C. P. Singh and R. Chari, *Dye Pigm.*, 2016, **126**, 110–117.
10 A. K. Diallo, C. Absalon, J. Ruiz and D. Astruc, *J. Am. Chem. Soc.*, 2011, **133**, 629–641.
11 J. C. Santos, F. Madrid-Moliné, C. A. Cisternas, F. Paul, C. A. Escobar, P. Jara-Ulloa and A. Trujillo, *Inorg. Chim. Acta*, 2018, **486**, 95–100.
12 G. Erbland, S. Abid, Y. Gisbert, N. Saffon-Merceron, Y. Hashimoto, L. Anderoni, T. Guérin, C. Kammerer and G. Rapenne, *Chem.–Eur. J.*, 2019, **25**, 16328–16339.
13 A. Hildebrandt, T. Rüffer, E. Erasmus, J. C. Swarts and H. Lang, *Organometallics*, 2010, **29**, 4900–4905.
14 G. Vives, A. Carella, J.-P. Launay and G. Rapenne, *Chem. Commun.*, 2006, 2283–2285.
15 J.-L. Fillaut, J. Lineares and D. Astruc, *Angew. Chem., Int. Ed. Engl.*, 1994, **33**, 2460–2462.
16 V. Mamane, I. Ledoux-Rak, S. Deveau, J. Zyss and O. Riant, *Synthesis*, 2003, **3**, 433–467.
17 V. Mamane, A. Gref and O. Riant, *New J. Chem.*, 2004, **28**, 585–594.
18 Y. Yu, A. D. Bond, P. W. Leonard, K. P. C. Vollhardt and G. D. Whitener, *Angew. Chem., Int. Ed.*, 2006, **45**, 1794–1799.
19 B. Alonso, I. Cuadrado, M. Morán and J. Losada, *J. Chem. Soc., Chem. Commun.*, 1994, 2575–2576.
20 Y. Yu, A. D. Bond, P. W. Leonard, U. J. Lorenz, T. V. Timofeeva, K. P. C. Vollhardt, G. D. Whitener and A. A. Yakovenko, *Chem. Commun.*, 2006, 2572–2574.
21 R. Misra, R. Sharma and S. M. Mobin, *Dalton Trans.*, 2014, **43**, 6891–6896.
22 R. Misra, R. Maragani, B. Pathak, P. Gautam and S. M. Mobin, *RCS Adv.*, 2015, **5**, 71046–71051.
23 K. Rahimpour and R. Teimuri-Mofrad, *Appl. Organomet. Chem.*, 2020, **34**, e5943.
24 P. Jutzi, C. Batz, B. Neumann and H.-G. Stammler, *Angew. Chem., Int. Ed. Engl.*, 1996, **35**, 2118–2121.
25 H. Butenschön, *Synthesis*, 2018, **50**, 3787–3808.
26 S. M. Rupf, G. Schröder, R. Sievers and M. Malischewski, *Chem.–Eur. J.*, 2021, **27**, 5125–5129.
27 K. N. Seneviratne, A. Bretschneider-Hurley and C. H. Winter, *J. Am. Chem. Soc.*, 1996, **118**, 5506–5507.
28 A. Bretschneider-Hurley and C. H. Winter, *J. Am. Chem. Soc.*, 1994, **116**, 6468–6469.
29 S. M. Rupf, I. S. Dimitrova, G. Schröder and M. Malischewski, *Organometallics*, 2022, **41**, 1261–1267.
30 Y.-H. Han, M. J. Heeg and C. H. Winter, *Organometallics*, 1994, **13**, 3009–3019.
31 S. Saito, S. Saito, T. Ohwada and K. Shudo, *Chem. Pharm. Bull.*, 1991, **39**, 2718–2720.
32 I. P. Beletskaya, K. P. Butin, A. N. Ryabtsev and O. A. Reutov, *J. Organomet. Chem.*, 1973, **59**, 1–44.
33 T.-P. Lin, R. C. Nelson, R. Wu, J. T. Miller and F. P. Gabbaï, *Chem. Sci.*, 2012, **3**, 1128–1136.
34 P. Nockemann, F. Schulz, D. Maumann and G. Meyer, *Z. Anorg. Allg. Chem.*, 2005, **631**, 649–653.
35 M. Nolte, I. Patenburg and G. Meyer, *Z. Anorg. Allg. Chem.*, 2007, **634**, 362–368.
36 M. Tsunoda and F. P. Gabbaï, *J. Am. Chem. Soc.*, 2000, **122**, 8335–8336.
37 M. R. Haneline, M. Tsunoda and F. P. Gabbaï, *J. Am. Chem. Soc.*, 2002, **124**, 3737–3742.
38 M. Fleischmann, J. S. Jones, G. Balázs and F. P. Gabbaï, *Dalton Trans.*, 2016, **45**, 13742–13749.
39 M. R. Haneline, R. E. Taylor and F. P. Gabbaï, *Chem.–Eur. J.*, 2003, **9**, 5188–5193.

40 T. J. Taylor, C. N. Burress and F. P. Gabbaï, *Organometallics*, 2007, **26**, 5252–5263.
41 G. E. Coates and A. Lauder, *J. Chem. Soc.*, 1965, 1857–1864.
42 T. S. Lobana, M. K. Sandhu, D. C. Povey and G. W. Smith, *J. Chem. Soc., Dalt. Trans.*, 1988, 2913–2914.
43 T. S. Lobana and M. K. Sandhu, *J. Chem. Soc., Dalt. Trans.*, 1989, 2339–2341.
44 G. Schwarzenbach and M. Schellenberg, *Helv. Chim. Acta*, 1965, **48**, 28–46.
45 A. J. Downs, E. A. V. Ebsworth and H. J. Emeléus, *J. Chem. Soc.*, 1962, 1254–1260.
46 W. Tyrra, D. Naumann and I. Pantenburg, *J. Fluorine Chem.*, 2003, **120**, 13–19.
47 P. Pyykkö and M. Straka, *Phys. Chem. Chem. Phys.*, 2000, **2**, 2489–2493.
48 A. Bondi, *J. Phys. Chem.*, 1964, **68**, 441–451.
49 S. L. Bell, R. D. Chambers, K. R. Musgrave and J. G. Thorpe, *J. Fluorine Chem.*, 1971, **1**, 51–57.
50 K. Züchner, T. J. Richardson, O. Glemser and N. Bartlett, *Angew. Chem., Int. Ed. Engl.*, 1980, **19**, 944–945.
51 A. Venker, T. Vollgraff and J. Sundermeyer, *Dalton Trans.*, 2018, **47**, 1933–1941.
52 N. G. Connelly and W. E. Geiger, *Chem. Rev.*, 1996, **96**, 877–910.
53 D. Astruc, *New J. Chem.*, 2011, **35**, 764–772.
54 R. Martinez and A. Tiripicchio, *Acta Cryst.*, 1990, **C46**, 202–205.
55 D. Astruc, M.-C. Daniel and J. Ruiz, *Chem. Commun.*, 2004, 2637–2649.
56 D. Astruc, C. Ornelas and J. Ruiz, *Chem.–Eur. J.*, 2009, **15**, 8936–8944.
57 J. Chen, J. Shan, Y. Xu, P. Su, L. Tong, L. Yuwen, L. Weng, B. Bao and L. Wang, *ACS Appl. Mater. Interfaces*, 2018, **10**, 34455–34463.
58 K.-Y. Pu, K. Li and B. Liu, *Adv. Mater.*, 2010, **22**, 643–646.
59 C. McCusker, J. B. Caroll and V. M. Rotello, *Chem. Commun.*, 2005, 996–998.
60 L.-I. Rodríguez, O. Rossell, M. Seco and G. Muller, *J. Organomet. Chem.*, 2007, **692**, 851–858.
61 D. M. L. Goodgame, S. Kealey, P. D. Lickiss and A. J. P. White, *J. Mol. Struct.*, 2008, **890**, 232–239.
62 M. A. Little, M. A. Halcrow, L. P. Harding and M. J. Hardie, *Inorg. Chem.*, 2010, **49**, 9486–9496.
63 C. S. Campos-Fernandez, R. Clerac, J. M. Koomen, D. H. Russell and K. R. Dunbar, *J. Am. Chem. Soc.*, 2001, **123**, 773–774.
64 C. S. Campos-Fernandez, B. L. Schottel, H. T. Chifotides, J. K. Bera, J. Bacsa, J. M. Koomen, D. H. Russell and K. R. Dunbar, *J. Am. Chem. Soc.*, 2005, **127**, 12909–12923.
65 I. D. Giles, H. T. Chifotides, M. Shatruk and K. R. Dunbar, *Chem. Commun.*, 2011, **47**, 12604–12606.
66 R. Lavendomme, T. K. Ronson and J. R. Nitschke, *J. Am. Chem. Soc.*, 2019, **141**, 12147–12158.
67 J. Yang, X.-Y. Chang, K.-C. Sham, S.-M. Yui, H.-L. Kwong and C.-M. Che, *Chem. Commun.*, 2016, **52**, 5981–5984.
68 H. Bock, A. John, C. Näther and Z. Havlas, *J. Am. Chem. Soc.*, 1995, **117**, 9367–9368.
69 A previous version of this manuscript has been deposited on a preprint server: S. M. Rupf, A. L. Moshtaha, and M. Malischewski, *ChemRxiv*, 2022, DOI: 10.26434/chemrxiv-2022-5rxlm.
70 Deposition numbers CCDC 2214089 ($[FeC_{10}(HgDMAP)_{10}][TFA]_{10}$), 2213962 ($[FeC_{10}(HgTHT)_{10}][SbF_6]_{10}\cdot 24$ MeCN) and 2213956 ($[FeCp_2(HgMeCN)_{10}][SbF_6]_{10}[MoF_6]\cdot 2SO_2\cdot 10$ HF) contain the supplementary crystallographic data for this paper. These data are provided free of charge by the joint Cambridge Crystallographic Data Centre and Fachinformationszentrum Karlsruhe Access Structures service.**https://www.ccdc.cam.ac.uk/structures**.